JOURNAL OF COMPUTATIONAL PHYSICS 35, 229–253 (1980)

A Particle-Fluid Numerical Model for Liquid Sprays*

JOHN K. DUKOWICZ

Theoretical Division, Group T-3, University of California, Los Alamos Scientific Laboratory, Los Alamos, New Mexico 87545

Received December 28, 1978

A numerical technique has been developed for computing the behavior of atomized non-evaporating liquid sprays injected into a gaseous environment. The same technique, however, is applicable to general incompressible flows containing particles or droplets. The method consists of a fully-interacting combination of Eulerian fluid and Lagrangian particle calculations. The interaction calculations are performed simultaneously and non-iteratively. A Lagrangian description of the particles avoids numerical diffusion, and allows individual attributes, such as particle size, composition, etc., to be statistically assigned for each particle. Numerical calculations and comparisons with experimental data are given for some sprays typical of diesel engine fuel injection.

1. INTRODUCTION

Many practical problems involve fluid flows containing particles or droplets. These problems range from the transport of particulate pollutants in the atmosphere to the spray injection of liquid fuels in internal combustion engines. For purposes of analysis, these problems may be divided into two classes. First, there are problems, such as the atmospheric pollutant problem, in which it may be assumed that the particles do not perturb the flow field. The solution then reduces to tracing particle trajectories in a known velocity field. Many examples of this treatment are available, such as Hotchkiss and Hirt [1] for the dispersion of atmospheric pollutants, and Gauvin, Katta, and Knelman [2] in the design of spray driers. Westbrook [3] has reported computations, based on the spray equation, for liquid fuel sprays in this regime.

In this paper, on the other hand, we are interested in problems, such as high-pressure fuel injection in an internal combustion engine, in which the spray carries sufficient momentum to entrain and set into motion the surrounding gas. In turn, the motion of the gas in the vicinity of the particles reduces the resistance to their motion and allows the spray to penetrate much further than would otherwise be the case. It is important, therefore, to account for the interaction between the particles and the gas. This interaction is of course always present, but it is particularly significant whenever the total mass and momentum of the particles is comparable to that of the gas, and

0021-9991/80/050229–25$02.00/0

when the size of the particles is sufficiently small so that the coupling of a particle to the gas is strong.

There have been several attempts to treat the problem of full coupling between the particles and the gas in a two- or three-dimensional flow field. Since diesel engine sprays appear to be completely vaporized a short distance away from the injector, theories [4, 5] have been developed based on the general similarity of these sprays to turbulent gas jets [6]. An example of a quasi-empirical model, also based on the assumption of a turbulent vapor jet, is the work of Chiu, Shahed, and Lyn [7]. A numerical technique, potentially applicable to liquid sprays, is the multiphase (commonly two-phase) technique [8, 9] incorporated in numerous codes used primarily for nuclear reactor safety analysis. In this technique, the droplets are considered to be a continuous fluid ("droplet phase") interpenetrating and interacting with the gas phase. However, in the common two-phase version the droplets are represented by a single average size, which generally is a severe simplification. In principle, this limitation may be removed by using several fields, each representing a class of particle sizes, to describe the spray. This approach, however, is very costly in terms of computer time and storage requirements. For spray applications, moreover, the numerical smearing of the spray due to the limited resolution of the mesh, especially in the vicinity of the injector, may not be acceptable. A related technique reported by Haselman and Westbrook [10] is based on a solution of the spray equation for the droplet distribution function.

An alternative procedure is to represent the spray by discrete particles, rather than by continuous distributions. This amounts to a statistical (Monte Carlo) formulation of the problem, since the finite number of particles used represents a sample of the total population of particles. Each computational particle is considered to represent a group of particles possessing the same characteristics such as size, composition, etc. The use of discrete particles eliminates the problems of numerical diffusion and of resolution in the vicinity of the injector. We have found that the required number of particles to achieve satisfactory accuracy is not excessive, and since frequently the particles are limited to a part of the mesh, the computing requirements are less severe.

One of the earliest implementations of this technique is contained in the YAQUI code described by Amsden and Hirt [11]. Few practical applications of this particle technique were made, however, because the method suffered from numerical difficulties in the particle–gas momentum exchange, requiring the use of prohibitively small time steps to achieve solution in the case of strong coupling between particles and the gas. For strong coupling, the momentum exchange terms should be treated implicity. In order to avoid iteration on these terms within a time step, YAQUI decoupled the calculation by treating the gas velocity in the momentum exchange terms explicitly. An implicit method to remove this difficulty is given by Crowe, Sharma, and Stock [12]. However, while preserving accuracy, the required iteration is time consuming. Their method also neglects the volume occupied by particles in a computational cell in comparison with the volume of the gas.

The method to be described in this paper differs from these previous attempts in many details, but principally in eliminating iteration for the particle–gas momentum

exchange and in accounting for particle volume displacement effects. It also differs by stressing a statistical, rather than a deterministic, approach to the modeling of sprays.

The technique is presently limited to particles whose size does not change (i.e., nonevaporating and nonburning sprays). This is not an inherent limitation of the method but it has been adopted to focus attention on the primary, hydrodynamic features of the method. In a subsequent publication we will describe the extension of the method to evaporating sprays.

2. Basic Equations

It will be assumed that no particle coalescence or particle breakup occurs. This implies that the particles are sufficiently dispersed that particle collisions are infrequent. The initial breakup of liquid sprays or jets is not considered. It is assumed that initial conditions for the particles are known. That is, the initial particle size distributions, positions, and velocities are independently specified.

This leads to two sets of equations, one set for the gas and the other for the particles. These equations will be coupled primarily by two mechanisms, the displacement of gas by the volume occupied by the particles and momentum interchange between particles and the gas. Because the particles are nonevaporating and nonburning, there is no mass exchange. Further, we assume that the gas or fluid containing the particles is incompressible with constant density ρ_g. This is a practical choice since most applications will deal with cases of highly subsonic flow. Generalization to compressible flow, however, presents no fundamental difficulties. Because of this constant density assumption, there is no need for energy equations or an equation of state.

2.1. *Gas Equations*

The continuity equation for the gas is given by [9]

$$\frac{\partial \theta}{\partial t} + \nabla \cdot \theta \mathbf{u}_g = 0, \tag{2.1}$$

where θ is the void fraction, or the fraction of the volume occupied by the gas, and $\mathbf{u}_g$ is the gas velocity. The presence of the void fraction in this equation accounts for the displacement effect of the particles. The definition of θ in terms of particle parameters will be given later.

The momentum equation takes the form [9]

$$\frac{\partial}{\partial t} \theta \mathbf{u}_g + \nabla \cdot \theta \mathbf{u}_g \mathbf{u}_g = \theta \mathbf{g} - \frac{\theta}{\rho_g} \nabla p + \nabla \cdot \theta \nu_g \nabla \mathbf{u}_g + \frac{1}{\rho_g} \mathbf{M}_p, \tag{2.2}$$

where $\mathbf{g}$ is the acceleration of gravity, p is the pressure, ν_g is the kinematic viscosity (or eddy viscosity if the flow is turbulent), and $\mathbf{M}_p$ is the term defining momentum

exchange with the particles, per unit volume. An alternative form of this equation can be obtained by subtracting out the continuity equation:

$$\frac{\partial}{\partial t}\mathbf{u}_g + \mathbf{u}_g \cdot \nabla \mathbf{u}_g = \mathbf{g} - \frac{1}{\rho_g}\nabla p + \frac{1}{\theta}\nabla \cdot \theta \nu_g \nabla \mathbf{u}_g + \frac{1}{\theta \rho_g}\mathbf{M}_p . \tag{2.3}$$

This is the form of the equation used in the numerical technique. The term containing $\mathbf{M}_p$ will be defined later.

2.2. *Particle Equations*

In a turbulent flow, the gas equations of the previous section are written in terms of the mean velocity $\mathbf{u}_g$. For particles, gas turbulence is important as a mechanism for diffusion; and it is convenient to write the instantaneous, rather than averaged, equations for the particles. To do this, we define the instantaneous gas velocity, $\mathbf{U}_g = \mathbf{u}_g + \mathbf{u}_g'$, where $\mathbf{u}_g'$ is the turbulent component of the gas velocity.

Each particle, individually labeled by subscript k, is assumed to obey the following equations:

$$\frac{d}{dt}\mathbf{x}_{pk} = \mathbf{u}_{pk} , \tag{2.4}$$

$$m_k \frac{d}{dt}\mathbf{u}_{pk} = m_k \mathbf{g} - \frac{m_k}{\rho_k}\nabla p + D_k[\mathbf{U}_g](\mathbf{U}_g - \mathbf{u}_{pk}), \tag{2.5}$$

where $\mathbf{x}_{pk}$ is the particle position, $\mathbf{u}_{pk}$ is its velocity, m_k is its mass, and ρ_k is its density. The notation $D_k[\mathbf{U}_g]$ is used to denote the drag function, evaluated using the velocity $\mathbf{U}_g$, which is the coefficient in the force acting on the particle due to its motion through the gas. It will be convenient to abbreviate the notation to D_k when referring to the drag function evaluated at the mean gas velocity $\mathbf{u}_g$ ($D_k \equiv D_k[\mathbf{u}_g]$). The time derivative is the Lagrangian derivative along the trajectory of the particle. The term containing the gradient of the pressure has been retained for consistency with two-fluid equations [9], even though it is generally a small term, of the order of the ratio of gas to particle densities compared to the corresponding term in the gas equation [Eq. (2.2)]. Several additional terms in the particle momentum equation of the same order of magnitude, such as the Bassett and virtual mass terms [13], have been neglected.

The drag function D_k depends on a variety of parameters such as the particle size and shape, local Reynolds number, and local particle density. We assume that particle density is sufficiently low that collective effects on particle drag are unimportant, and we make the common assumption that the particles are spherical with radius r_k. The drag function of a nonevaporating sphere is a well-known function of the Reynolds number, but for computational reasons we have approximated it by the simplified expression

$$D_k = 6\pi \mu_g r_k + \tfrac{1}{2}\pi r_k^2 \rho_g C_D \,|\, \mathbf{u}_g - \mathbf{u}_{pk} \,|\, , \tag{2.6}$$

where μ_g is the gas viscosity. The first term represents the Stokes drag, valid in the limit of a very low Reynolds number,

$$2r_k \mid \mathbf{u}_g - \mathbf{u}_{pk} \mid \rho_g/\mu_g < 1,$$

and the second term is the form drag, evaluated using the drag coefficient $C_D = 0.4$, which dominates in the limit of very large Reynolds number. The particle mass is given by

$$m_k = \tfrac{4}{3}\pi r_k^3 \rho_k \,. \tag{2.7}$$

It is sometimes more convenient to consider the effect of turbulence on the particles to be due to a force $\mathbf{f}_{pk}$, in which case the momentum equation is written

$$m_k \frac{d}{dt}\mathbf{u}_{pk} = m_k \mathbf{g} - \frac{m_k}{\rho_k}\nabla p + D_k(\mathbf{u}_g - \mathbf{u}_{pk}) + \mathbf{f}_{pk}\,, \tag{2.8}$$

where the turbulence force $\mathbf{f}_{pk}$ is given by

$$\mathbf{f}_{pk} = D_k[\mathbf{U}_g](\mathbf{U}_g - \mathbf{u}_{pk}) - D_k(\mathbf{u}_g - \mathbf{u}_{pk}). \tag{2.9}$$

The terms in the gas equations [Eqs. (2.1)–(2.3)] dependent on the particles have not yet been defined. Taking ensemble averages, we can write

$$\theta = 1 - \sum_k \langle \tfrac{4}{3}\pi r_k^3 \delta(\mathbf{x} - \mathbf{x}_{pk})\rangle \tag{2.10}$$

and

$$\mathbf{M}_p = -\sum_k \langle D_k[\mathbf{U}_g](\mathbf{U}_g - \mathbf{u}_{pk})\,\delta(\mathbf{x} - \mathbf{x}_{pk})\rangle, \tag{2.11}$$

where $\delta(\mathbf{x})$ is the three-dimensional Dirac delta function. For numerical purposes, the ensemble averages are replaced by volume averages, as explained in the Appendix. The Appendix also contains a discussion of the relationship between the particle description and the continuum description employed in the multifluid equations.

3. Numerical Technique

The numerical algorithm for the solution of the gas equations is based on the SOLA code [15]. This is a simplified, incompressible, two-dimensional flow code available from the National Energy Software Center (formerly Argonne Code Center). Numerous offshoots of the basic code have been constructed but all are based on a mesh composed of rectangular cells illustrated in Fig. 1. The version of the code actually used differs from the one described [15] in that it has variable mesh line spacing. Velocities are defined in the middle of cell faces. Thus, there are two staggered

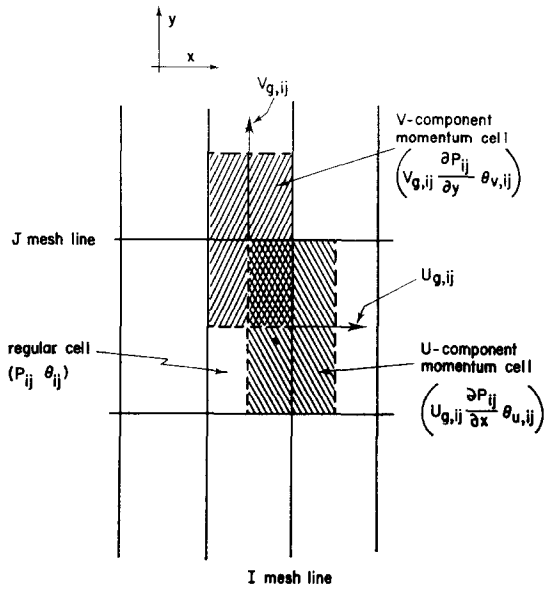

FIG. 1. Typical cells and variables associated with the finite-difference mesh.

meshes associated with the respective velocity components, and the corresponding cells, called momentum cells, are indicated by dashed lines in Fig. 1.

These computational cells act as control volumes for the dependent variables associated with the basic equations. The regular cells are the control volumes for the mass continuity equation. Variables associated with them are the pressure p_{ij} and the void fraction θ_{ij}. The momentum cells are the control volumes for the momentum equations, and the associated variables are $u_{g,ij}$ and $v_{g,ij}$ and the components of the pressure gradient ∇p. To a first approximation, these variables are assumed to be constant within their respective cells.

Spatial differencing in a rectangular mesh is generally straightforward and is described in the SOLA report [15]. The temporal differencing contains the essence of the present technique and will be described in some detail. We will use superscripts to denote time levels such that, for example,

$$p_{ij}^{n} = p_{ij}(t^{n}) \tag{3.1}$$

and

$$p_{ij}^{n+1} = p_{ij}(t^{n} + \Delta t) = p_{ij}(t^{n+1}). \tag{3.2}$$

We shall also use a time-splitting procedure employing intermediate time levels denoted by superscripts such that

$$t^{n} < t^{T} < t^{2T} < t^{3T} < t^{n+1}. \tag{3.3}$$

Subscripts denoting cells will be omitted, since in general it will be obvious from the variable itself to which type of cell it is referred. Frequently, to simplify notation, vector equations will be written for the x-component only.

Individual particles will be denoted by subscript k. Quantities associated with each particle will be its radius r_k, position $\mathbf{x}_k$, velocity $\mathbf{u}_{pk}$, and number of particles in the group N_{pk}. The density of each particle may be different (ρ_k), although for the present it is assumed to be constant ρ_p.

3.1. *Void Fraction and Continuity Equation*

Knowing the position of each particle at time t^{n+1} the void fraction is calculated using Eq. (2.10). For each regular cell the void fraction is

$$\theta_{ij}^{n+1} = 1 - \frac{4\pi}{3V_{ij}} \sum_k N_{pk} r_k^3, \tag{3.4}$$

where the summation is over all particles in regular cell (ij) and V_{ij} is the volume of that cell. The void fraction is assumed to be centered in the cell; values at cell faces are obtained by linear interpolation.

The continuity equation [Eq. (2.1)], omitting cell subscripts, is differenced as follows:

$$\frac{\theta^{n+1} - \theta^n}{\Delta t} + \nabla \cdot \theta_u^{n+1} \mathbf{u}_g^{n+1} = 0, \tag{3.5}$$

where θ_u^{n+1} refers to a cell-face void fraction, associated with a momentum cell, obtained by interpolation.

3.2. *Momentum Exchange Term and Momentum Equations*

Consider, for example, a momentum cell associated with the velocity component $u_{g,ij}$. The argument for the velocity component $v_{g,ij}$ is entirely analogous. For particles within this cell the momentum exchange term [Eq. (2.11)] is written

$$M_{p,x}^{n+1} = -\frac{1}{V_u} \sum_k N_{pk} D_k^{2T}[\mathbf{U}_g](U_g^{n+1} - u_{pk}^{n+1}), \tag{3.6}$$

omitting the cell subscript, where V_u is the momentum cell volume. Notice that the term is linearly implicit in the velocities, in the sense that while the drag function is evaluated at some intermediate time level $2T$, to be defined leter, the relative velocity factor is evaluated at the time t^{n+1}. In order to evaluate this term it is necessary to consider the particle momentum equation, which is differenced as follows:

$$\frac{u_{pk}^{n+1} - u_{pk}^n}{\Delta t} = g_x - \frac{1}{\rho_p} \frac{\partial p^{n+1}}{\partial x} + \frac{D_k^{2T}[\mathbf{U}_g]}{m_k} (U_g^{n+1} - u_{pk}^{n+1}). \tag{3.7}$$

Rearranging terms, this equation can be written as

$$D_k^{2T}[\mathbf{U}_g](u_{pk}^{n+1} - U_g^{n+1}) = \frac{D_k^{2T}(u_{pk}^n - U_g^{n+1})}{1 + \Delta t\, D_k^{2T}/m_k} + \frac{\Delta t\, D_k^{2T}}{1 + \Delta t\, D_k^{2T}/m_k}\left(g_x - \frac{1}{\rho_p}\frac{\partial p^{n+1}}{\partial x}\right), \tag{3.8}$$

where we have used the short notation $D_k^{2T} \equiv D_k^{2T}[\mathbf{U}_g]$. Now, summing over all particles in the momentum cell and recalling that u_g^{n+1} and $\partial p^{n+1}/\partial x$ are assumed to be constant within the cell, we obtain

$$\sum_k N_{pk} D_k^{2T}[\mathbf{U}_g](u_{pk}^{n+1} - U_{\cdot}^{n+1}) = \sum_k \frac{N_{pk} D_k^{2T}(u_{pk}^n - u_g')}{1 + \Delta t\, D_k^{2T}/m_k} + \left[\left(g_x - \frac{1}{\rho_p}\frac{\partial p^{n+1}}{\partial x}\right)\Delta t - u_g^{n+1}\right]\sum_k \frac{N_{pk} D_k^{2T}}{1 + \Delta t\, D_k^{2T}/m_k}.$$

If we define

$$R_u^{2T} \equiv \frac{1}{\rho_g \theta_u^{n+1} V_u}\sum_k \frac{N_{pk} D_k^{2T}}{1 + \Delta t\, D_k^{2T}/m_k}(u_{pk}^n - u_g'), \tag{3.10}$$

$$S_u^{2T} \equiv \frac{1}{\rho_g \theta_u^{n+1} V_u}\sum_k \frac{N_{pk} D_k^{2T}}{1 + \Delta t\, D_k^{2T}/m_k}, \tag{3.11}$$

where θ_u^{n+1} is the void fraction associated with the momentum cell, the momentum exchange term becomes

$$M_{p,x}^{n+1} = \rho_g \theta_u^{n+1}\left[\left(g_x - \frac{1}{\rho_p}\frac{\partial p^{n+1}}{\partial x}\right)\Delta t\, S_u^{2T} - u_g^{n+1} S_u^{2T} + R_u^{2T}\right]. \tag{3.12}$$

The parameters R_u^{2T} and S_u^{2T} are momentum cell quantities that depend on explicitly available particle information. They vanish when particles are absent from the cell.

The x-component of the gas momentum equation [Eq. (2.3)] is therefore temporally differenced as follows:

$$\frac{u_g^{n+1} - u_g{}^n}{\Delta t} + F_x{}^n = g_x - \frac{1}{\rho_g}\frac{\partial p^{n+1}}{\partial x} + \left(g_x - \frac{1}{\rho_p}\frac{\partial p^{n+1}}{\partial x}\right)\Delta t\, S_u^{2T} - u_g^{n+1} S_u^{2T} + R_u^{2T}, \tag{3.13}$$

where

$$F_x{}^n \equiv \mathbf{u}_g{}^n \cdot \nabla u_g{}^n - \frac{1}{\theta_u^{n+1}}\nabla \cdot \theta^{n+1} \nu_g \nabla u_g{}^n. \tag{3.14}$$

The set of equations to be solved is composed of Eqs. (3.5), (3.7), and (3.13),

together with the corresponding v-component equations. The equations are implicit in the pressure and partly implicit in the velocities. The continuity equation [Eq. (3.5)] and the gas momentum equation [Eq. (3.13)] are solved by iteration in analogy with the MAC method [16]. The particle momentum equation [Eq. (3.7)] is solved directly once p^{n+1} and $\mathbf{u}_g^{n+1}$ are known. Note that the procedure defined by Eqs. (3.8)–(3.14) has eliminated the need to iterate between the particle and gas equations. The actual computational procedure is described next.

3.3. *Computational Procedure*

The computational cycle starts by introducing new particles into the mesh as a result of injection, or transport through inflow. The procedure for injecting particles in the case of a spray is described in the following section. The particles are then transported using the explicit equations

$$\frac{\mathbf{x}_{pk}^{n+1} - \mathbf{x}_{pk}^{n}}{\Delta t} = \mathbf{u}_{pk}^{n}. \tag{3.15}$$

Since the particle position has changed, the void fraction θ^{n+1} is updated using Eq. (3.4), in those cells where a particle has left or has entered. At the same time, particles leaving the computing mesh, or otherwise disappearing, are removed and all particle arrays are repacked.

The equations that have to be solved next, simultaneously, are the gas and particle momentum equations:

$$\frac{u_g^{n+1} - u_g{}^n}{\Delta t} + F_x{}^n = g_x - \frac{1}{\rho_g}\frac{\partial p^{n+1}}{\partial x} + \left(g_x - \frac{1}{\rho_p}\frac{\partial p^{n+1}}{\partial x}\right)\Delta t\, S_u^{2T} - u_g^{n+1} S_u^{2T} + R_u^{2T} \tag{3.13}$$

and

$$\frac{u_{pk}^{n+1} - u_{pk}^{n}}{\Delta t} = g_x - \frac{1}{\rho_p}\frac{\partial p^{n+1}}{\partial x} + \frac{D_k^{2T}}{m_k}(U_g^{n+1} - u_{pk}^{n+1}). \tag{3.7}$$

We shall employ a splitting procedure, which, while preserving the original equations, will solve them in a number of stages.

The purpose of the first and second stages is to predict explicitly new-time gas and particle velocities in order to calculate D_k^{2T}, and therefore S_u^{2T} and R_u^{2T}. We first calculate intermediate gas and particle velocities, accounting explicitly for all forces, except for particle interactions and turbulence, using the following equations:

$$\frac{u_g{}^T - u_g{}^n}{\Delta t} + F_x{}^n = g_x - \frac{1}{\rho_g}\frac{\partial p^n}{\partial x} \tag{3.16}$$

and

$$\frac{u_{pk}^T - u_{pk}^n}{\Delta t} = g_x - \frac{1}{\rho_p}\frac{\partial p^n}{\partial x}. \tag{3.17}$$

These temporary velocities are used to evaluate a temporary drag function $D_k{}^T$, using Eq. (2.6), and then to calculate the particle interaction terms $S_u{}^T$ and $R_u{}^T$, from Eqs. (3.10) and (3.11), neglecting turbulence ($u_g' = 0$). A second approximation to the gas and particle velocities, approximately accounting for particle interactions, is now obtained using the following equations:

$$\frac{u_g^{2T} - u_g{}^T}{\Delta t} = \left(g_x - \frac{1}{\rho_p}\frac{\partial p^n}{\partial x}\right)\Delta t\, S_u{}^T - u_g^{2T} S_u{}^T + R_u{}^T \tag{3.18}$$

and

$$\frac{u_{pk}^{2T} - u_{pk}^T}{\Delta t} = \frac{D_k{}^T}{m_k}(u_g^{2T} - u_{pk}^{2T})\,. \tag{3.19}$$

Having both gas and particle velocities at stage $2T$ makes it possible to calculate D_k^{2T}, the final approximation to the drag function. The drag function at this stage should contain the effects of turbulence (Section 2.2). We therefore calculate $\mathbf{u}_g'$ (methods for estimating $\mathbf{u}_g'$ or $\mathbf{f}_{pk}$ will be discussed in Section 3.5), and proceed to calculate D_k^{2T}, and hence S_u^{2T} and R_u^{2T}. At this stage it is also convenient (since turbulent velocities $\mathbf{u}_g'$ are available) to update particle velocities for turbulence:

$$\frac{u_{pk}^{3T} - u_{pk}^n}{\Delta t} = \frac{D_k^{2T}}{m_k}(u_g^{2T} + u_g' - u_{pk}^{3T}). \tag{3.20a}$$

The gas velocity is next explicitly updated for particle interactions:

$$\frac{u_g^{3T} - u_g{}^T}{\Delta t} = \left[g_x - \frac{1}{\rho_p}\frac{\partial p^n}{\partial x}\right]\Delta t\, S_u^{2T} - u_g^{3T} S_u^{2T} + R_u^{2T}. \tag{3.20b}$$

This leaves the implicit portion of the momentum equation, which is conveniently written as follows:

$$u_g^{n+1} - u_g^{3T} = -\frac{\Delta t}{\rho_g}\left[\frac{1 + (\rho_g/\rho_p)\,\Delta t\, S_u^{2T}}{1 + \Delta t\, S_u^{2T}}\right]\frac{\partial}{\partial x}(p^{n+1} - p^n). \tag{3.21}$$

This equation, together with the continuity equation [Eq. (3.5)], forms the basis for a MAC-type pressure iteration to obtain final values of $\mathbf{u}_g^{n+1}$ and p^{n+1}.

Following the iteration, the particle velocities are updated to the final time level using the equation:

$$\frac{u_{pk}^{n+1} - u_{pk}^{3T}}{\Delta t} = g_x - \frac{1}{\rho_p}\frac{\partial p^{n+1}}{\partial x} + \frac{D_k^{2T}}{m_k}(u_g^{n+1} - u_g^{2T} - u_{pk}^{n+1} + u_{pk}^{3T}). \tag{3.22}$$

This brings all velocities to the final level. The time is now incremented and the cycle repeated with the new velocities.

3.4. *Injection of Particles*

Each particle injected or entering the mesh must be assigned a velocity $\mathbf{u}_{pk}$, a radius r_k, and the number of particles in the group N_{pk}. Let the number of computational particles injected per cell per time step be K. The radius of each particle is then chosen from a uniform random distribution in the range

$$0 < r_k < r_{\max} \qquad \text{for} \quad 1 < k < K.$$

If the particle mass flow into the cell is Q, we can write the following equations defining N_{pk}:

$$\sum_{k=1}^{K} N_{pk} m_k = Q\Delta t \tag{3.23}$$

and

$$f_r(r_k) = \alpha N_{pk} \Big/ \sum_{l=1}^{K} N_{pl}\,, \tag{3.24}$$

where α is a proportionality constant and $f_r(r)$ is the initial particle size distribution function. These two relationships [Eqs. (3.23)–(3.24)] are sufficient to determine N_{pk}. Note, however, that more than one particle per cell must be injected ($K > 1$) in order to develop a distribution of particles which approximates the specified size distribution function $f_r(r_k)$.

We assume that the particle velocity distribution is independent of the size distribution. The velocity distribution is very much problem dependent. As an illustration, the following procedure was employed for modeling a simple, single-hole spray injector. Assume that the spray is injected in the vertical direction. If the mass flow Q is known, the magnitude of the injection velocity is

$$V = \frac{4}{\pi} \frac{Q}{\rho_p d^2}\,, \tag{3.25}$$

where d is the diameter of the injector orifice. Of course, Q may be time dependent. Alternatively, if the pressure drop across the nozzle is known, then

$$V = C_Q \left(\frac{2\Delta p}{\rho_p}\right)^{1/2}, \tag{3.26}$$

where C_Q is the discharge coefficient of the nozzle and Δp is the pressure drop. The transverse velocity is derived in terms of the initial spray angle using the relationship

$$\text{Max}(u_{pk}) = V \tan\theta, \tag{3.27}$$

where θ is the half-angle of the initial portion of the spray cone. Transverse velocities

are then assigned to individual particles from a uniform random distribution in the range $0 < u_{pk} < \text{Max}(u_{pk})$. Since the magnitude of the droplet velocity is V, this determines both components of velocity. The initial spray angle must be provided for the injector in question; however, some guidance is available. For conditions in the range of interest for spray fuel injection, it is found [17] that

$$\tan \theta = A \left(\frac{\rho_g}{\rho_p}\right)^{1/2}, \tag{3.28}$$

where A is a constant dependent on the nozzle used. Therefore, it may be adequate to characterize the nozzle by the single parameter A.

3.5. *Turbulent Diffusion of Particles*

Turbulence is a very complex phenomenon; in general it will not be possible to deal with it, or its effects on the particles, in any detail. The effect of turbulence on the particles is formally accounted for by the presence of the term $\mathbf{f}_{pk}$ in the particle momentum equation [Eq. (2.8)]. The principal effect of interest is particle diffusion [18]. With this in mind, there are two relatively simple techniques which may be employed to model $\mathbf{f}_{pk}$.

An effective numerical technique for computing the turbulent transport of particulates is given by Hotchkiss and Hirt [1]. They assume that a diffusion equation exists for particle concentration, and a turbulent particle diffusivity D_T is known. Each computational particle is assumed to diffuse about its position at the start of a time step. The resulting particle concentration, which is Gaussian, forms a distribution function for the location of the particle. Particle positions are randomly selected from within this distribution, such that on each time step the diffusional increment in particle position is

$$\Delta \mathbf{x}_{pk} = (4D_T \Delta t)^{1/2} \operatorname{sgn}(X, Y) \operatorname{erf}^{-1}(|X|, |Y|), \tag{3.29}$$

where X and Y are random variables, associated with the x- and y-coordinates, selected from a uniform distribution in the range $-1, < X, Y < 1$. This is equivalent to selecting the following random particle force on each time step:

$$\mathbf{f}_{pk} = m_k \frac{\Delta \mathbf{x}_{pk}}{\Delta t^2}. \tag{3.30}$$

The turbulent diffusion constant D_T may be estimated by the method of Margolin [18], for example, and in general this will require turbulence modeling to evaluate the properties of the turbulence field.

An alternative possibility is to attempt to model the diffusion directly, as a random walk of the particles acted on by the turbulent gas velocity field. We assume that

fluid turbulence is isotropic and has a Gaussian distribution in velocity. Given the turbulent kinetic energy q, where

$$q = \overline{\mathbf{u}_g' \cdot \mathbf{u}_g'}, \tag{3.31}$$

random instantaneous turbulent velocities may be selected from the distribution as follows:

$$\mathbf{u}_g' = g^{1/2} \operatorname{sgn}(X, Y) \operatorname{erf}^{-1}(|X|, |Y|), \tag{3.32}$$

where, as before, X and Y are random variables selected for a uniform distribution in the range $-1 < X, Y < 1$. To complete the discription, the relevant turbulence time scale τ is required. The velocity $\mathbf{u}_g'$ is assumed to act for a time equal to τ. The random particle force is then estimated using Eq. (2.9), or the turbulent component $\mathbf{u}_g'$ may be simply added to the gas velocity in the particle momentum equation [Eq. (3.20a)]. Again, turbulence modeling is required to estimate q and τ.

Numerically, the two techniques are equivalent with a suitable choice of D_T. An elementary analysis suggests that the second method produces particle diffusion corresponding to

$$D_T \sim \frac{1}{6}\left(\frac{D_k}{m_k}\right)^2 q\tau^3. \tag{3.33}$$

It is clear that this type of treatment will fail to account for effects due to the presence of one or more particles within the same turbulent eddy. Such a level of description is unwarranted, however, since the principal aim is to describe the particle diffusion and this is already adequately defined by the parameter D_T.

4. Numerical Results

4.1. *Single-Orifice Diesel Spray*

The initial application of the present technique has been the modeling of fuel injection sprays. It would be desirable to compute sprays for which experimental data are available so that a direct comparison could be made. Unfortunately, experiments which provide sufficient data to specify the spray do not appear to exist. The experiments of Hiroyasu and Kadota [19, 20] come closest to providing such data and were therefore chosen to provide the basis for the following computations. To specify the spray, information is needed on the injected droplet size distribution, as well as the velocity distribution, which in general will be time dependent. For computational purposes these data had to be estimated, and in some cases drastic approximations had to be made.

The experiment of Hiroyasu and Kadota consisted of injecting diesel fuel oil, using a diesel-type injection system, into a high-pressure low-temperature gaseous environment. The objective of the experiment was to evaluate droplet size distributions for a

TABLE I

Experimental Spray Data [19]

Fuel	Diesel fuel oil, $\rho_p = 840$ kg/m^3
Pump	Bosch PE6A60B
Pump speed	500 rpm
Nozzle	Single-hole orifice (diameter $d = 0.3$ mm)
Nozzle opening pressure	$P_{in} = 9.9$ MPa
Ambient gas	Nitrogen
Gas pressure	0.1–5.0 MPa
Gas temperature	20~ 25°C

number of injectors and for a range of experimental parameters. Because of the low ambient temperature and the low volatility of diesel oil, it is felt that evaporation was not a factor in this experiment. The experimental conditions for which numerical calculations were made are listed in Table I.

Since injection velocity was not measured, it was estimated using Eq. (3.26) with $C_O = 0.8$, and assuming that nozzle pressure was equal to the valve opening pressure of 9.9 MPa. Valve opening was assumed to be instantaneous, and the valve was assumed to stay open for the duration of the calculation. This is not entirely realistic. Examples of oscilloscope traces of nozzle inlet pressure and nozzle needle lift [19, 20] show that they are not time independent, and therefore the calculations neglect the initial injection system dynamics. Transverse injection velocities were estimated on the basis of Eq. (3.28), using $A = 0.4$, which approximately corresponds to the experimental data for initial spray angle. Eddy viscosity was estimated using a value appropriate to a turbulent gaseous jet [21]:

$$\nu_g = 0.0161\,(K_m)^{1/2}, \tag{4.1}$$

where

$$K_m = 2\pi \int_0^\infty v^2 x\, dx = \tfrac{1}{4}\pi d^2\, V^2, \tag{4.2}$$

where d is the orifice diameter and V is the droplet injection velocity. No attempt was made to calculate particle diffusion accurately. Particle turbulence was modeled using the second method of Section 3.5, arbitrarily assuming $q = 0.1\mathbf{u}_g \cdot \mathbf{u}_g$ and $\tau = \Delta t$.

The droplet size distribution was measured in the experiment using a collection system located about 65 cm downstream of the injector. It was found that all the data were fitted by a size distribution function of the form:

$$f_r(r) = \frac{6}{D_{32}} \exp\left(\frac{-6r}{D_{32}}\right), \tag{4.3}$$

where D_{32} is the Sauter mean diameter, defined by

$$D_{32} = \int_0^\infty D^3 f_r(r)\, dr \Big/ \int_0^\infty D^2 f_r(r)\, dr, \tag{4.4}$$

where D is the droplet diameter ($D = 2r$). Therefore, the distribution is characterized by the single parameter D_{32}. Very little variation in D_{32} was observed among the three types of nozzles tested. A reduction of D_{32} with radial distance away from the spray axis was observed. For computational purposes, the measured value of D_{32} closest to the axis was taken to be the reference value for the spray.

However, the measured value of D_{32} is unlikely to be characteristic of the droplet size in the vicinity of the injector. For example, for the spray injected into a back pressure of $P_b = 3.0$ MPa (30 atm), simple droplet stability considerations based on the Weber number criterion:

$$\frac{\rho_g \,|\, \mathbf{u}_g - \mathbf{u}_p \,|^2 r_p}{\sigma_p} \approx 10,$$

where σ_p is the droplet surface tension, and assuming a representative relative velocity of 40 m/s (maximum injection velocity ~100 m/s), suggest a stable droplet radius to be about 5 μ, compared to the measured Sauter mean radius of 50 μ. This implies that agglomeration occurs somewhere downstream of the injector, or in the sample collection apparatus. For computational purposes, the measured size distribution function was retained, but the measured reference Sauter mean diameter was reduced by a constant factor of 10 to more nearly represent the distribution in the vicinity of the injector. The resulting parameters, defining the computed sprays, are given in Table II.

The spray was assumed to be axially symmetric, and the computation was carried out in cylindrical coordinates. The mesh and a typical computed velocity vector plot and particle plot are shown in Fig. 2. The axis of symmetry is located vertically in the center of the mesh. For good accuracy it was found necessary to refine the mesh near the spray axis, as shown. This is because of the large velocity gradients near the axis,

TABLE II

Estimated Spray Data

Gas pressure (MPa)	Injection velocity (m/s)	Transverse velocity (m/s)	Gas density (kg/m³)	Mass flow (kg/s)	Sauter mean radius(SMR) (μ)	Eddy viscosity (m²/s)
0.1	122.2	1.79	1.123	0.007256	5.0	7.1×10^{-4}
1.1	115.8	5.61	12.36	0.006876	4.3	6.4×10^{-4}
3.0	102.54	8.19	33.7	0.006088	5.0	5.0×10^{-4}
5.0	86.41	8.89	56.17	0.005131	5.5	3.6×10^{-4}

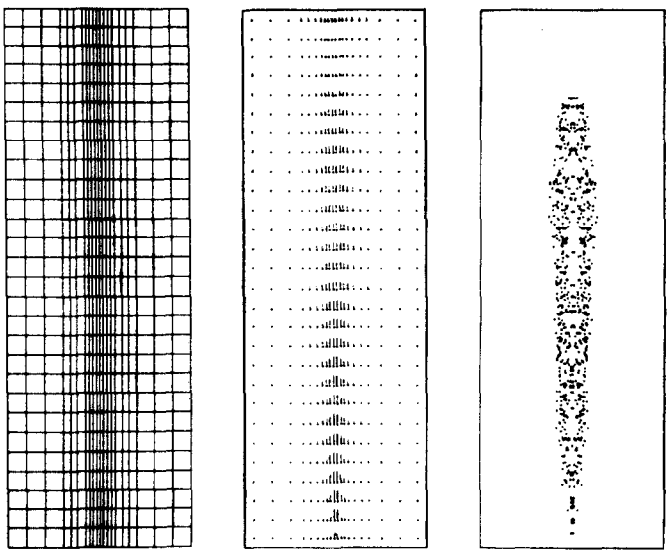

FIG. 2. Representative results from a spray calculation ($P_b = 3.0$ MPa, $t = 2.5$ ms). (a) Mesh; (b) gas velocity vectors; (c) Particle distribution.

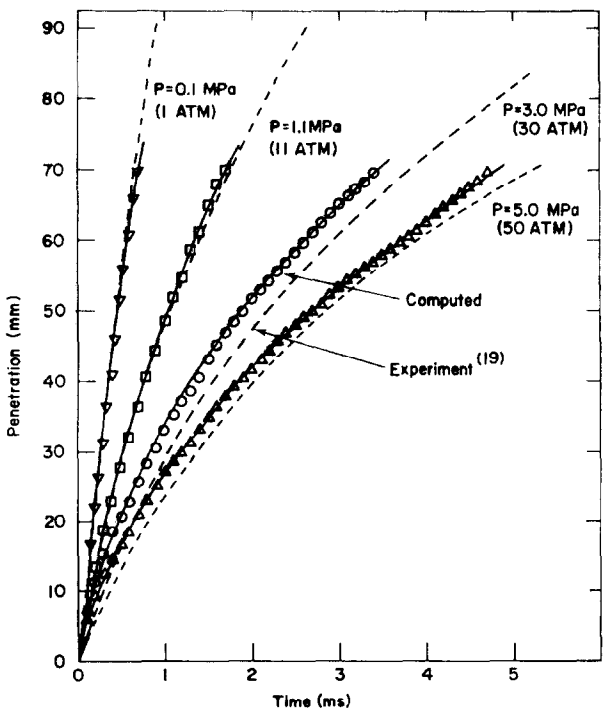

FIG. 3. Comparison of computed spray penetration with experimental data of Hiroyasu and Kadota [19].

and because large cells imply low gas velocity for a given momentum, and therefore result in unrealistically high drag between the particles and the gas. The velocity plot shows the gas velocities to be essentially confined to the vicinity of the spray, except near the injector where gas entrainment is more pronounced.

The computed penetration of the tip of the spray as a function of time is compared with the experimental data [19] in Fig. 3, for four levels of ambient gas pressure. In spite of the uncertainties in droplet size, injection velocity, and mass flow, the overall agreement is remarkably good, both for the magnitude of the penetration and the shape of the curves, especially in view of the fact that spray penetration is a sensitive function of the spray dynamics. We have made calculations to show that single droplets of a size characteristic of these sprays exhibit minimal penetration under these conditions. For example, an 11-μ-diameter droplet will penetrate about 2.1 mm after 5 ms in the case of ambient pressure $P_b = 5.0$ MPa. This emphasizes the great importance of the spray–gas interaction, and the resulting entrainment of the gas into the spray, in determining the spray penetration.

The effect of initial injector system dynamics is illustrated in Fig. 4. Examples of oscilloscope traces of nozzle inlet pressure and nozzle needle lift are given in [20] for the case of ambient pressure $P_b = 1.1$ MPa. These traces were used to account approximately for time-varying injection pressure and mass flow. The injection velocity was assumed to vary injection pressure according to Eq. (3.26). The mass

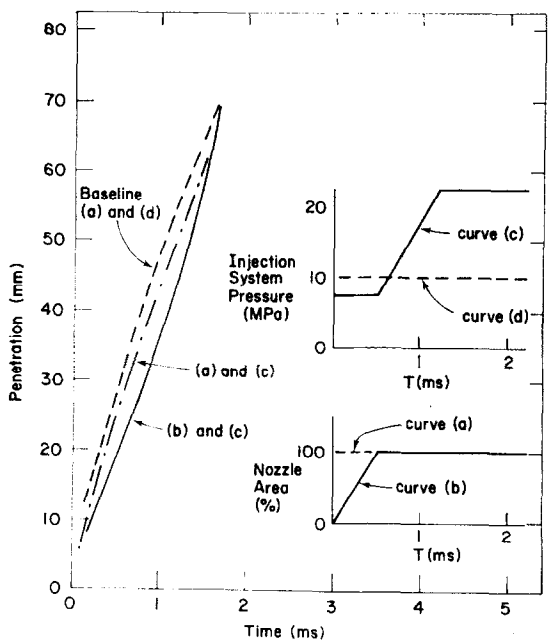

FIG. 4. The effect of time-varying injection system pressure and effective nozzle area on the initial shape of the spray penetration curve ($P_b = 1.1$ MPa).

flow was estimated in two ways. In the first case, it was assumed that the effective nozzle area is proportional to the needle lift, which therefore serves as a factor multiplying the mass flow given by Eq. (3.25). In the second case, because of the very small nozzle area, it was assumed that the nozzle is fully opened as soon as the needle begins to lift. The resulting spray penetration for these two cases is compared with the baseline spray (conditions listed in Table II and plotted in Fig. 3). The approximate injection pressure and nozzle lift function used in the calculation are also shown in the figure. Both these parameters significantly affect the penetration, especially in the initial portion of the spray trajectory, and therefore should be modeled for an accurate description of the spray.

4.2. *Monodisperse Spray*

One of the main limitations of the two-phase technique [8, 9], described earlier, is its inability to account for more than a single droplet size. It is interesting, therefore, to look at the behavior of monodisperse sprays in order to evaluate this limitation. Figure 5 shows a series of particle plots comparing the behavior of monodisperse sprays for the case $P_b = 1.1$ MPa at 1.0 ms after the start of injection The first four plots are monodisperse sprays containing particles of radius 2.1, 4.3, 6.4, and 8.6 μ, respectively. The fifth plot is the corresponding polydisperse spray with particle radii in the range 0–8.6 μ, distributed according to Eq. (4.3) with a Sauter mean radius

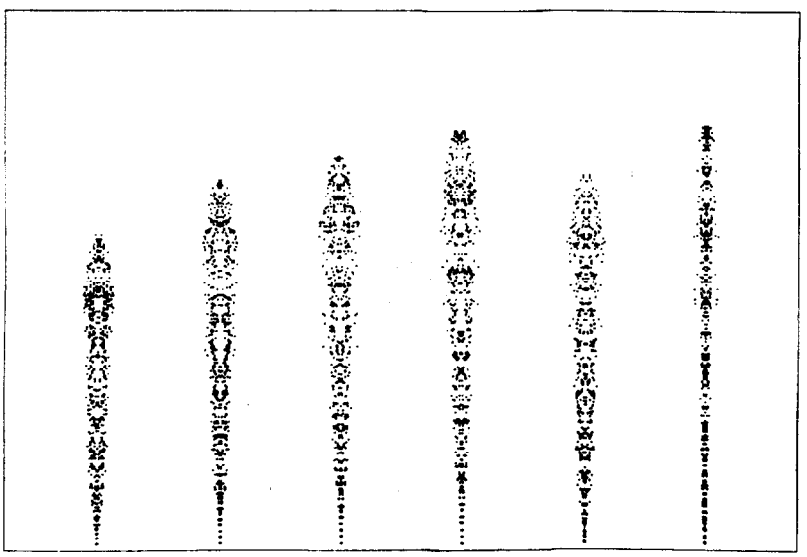

FIG. 5. Particle plots illustrating the effect of droplet size in a monodisperse spray, and the effect of particle turbulence on the shape and penetration of the spray ($P_b = 1.1$ MPa, $t = 1.0$ ms). (a) Monodisperse, $r_p = 2.1$ μ; (b) monodisperse, $r_p = 4.3$ μ; (c) monodisperse, $r_p = 6.4$ μ; (d) monodisperse, $r_p = 8.6$ μ; (e) polydisperse, $r_p = 0$–8.6 μ; SMR $= 4.3$ μ; (f) Polydisperse with no particle turbulence, $r_p = 0$–8.6 μ, SMR $= 4.3$ μ.

(SMR) of 4.3 μ. The monodisperse sprays show widely different penetration, although, coincidentally, the penetration of the polydisperse spray with SMR = 4.3 μ is approximately the same as the penetration of the monodisperse spray with the same droplet radius. The last plot shows the same polydisperse spray, but without particle turbulence. It can be clearly seen that the turbulence produces diffusion of the particles and increases the apparent spray angle. It also reduces the penetration of the spray, presumably because the more widely dispersed spray is able to transfer its momentum to more of the gas, reducing gas velocity, and therefore increasing the drag on the spray. In many calculations it is possible to discern a characteristic "cap" forming at the head of the spray, especially in spray patterns without particle turbulence. The cap is composed of droplets which reach the outer periphery of the spray, where they are left behind because of their low velocity. With particle turbulence the cap is less apparent because turbulent diffusion smears out such features; however, these slow droplets are still present in the outer periphery of the spray.

4.3. *Effect of Varying Particle Number*

The number of particles injected per cell per time-step (K) is a free parameter. Since the mass flux is fixed, varying K implies a change in N_{pk}, the number of particles in the group represented by a computational particle. Increasing the number of

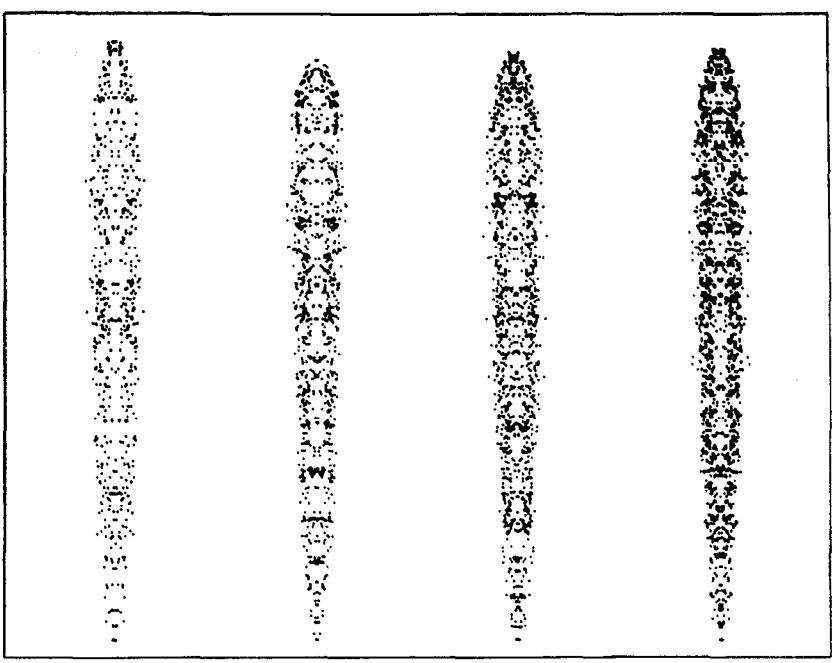

FIG. 6. Particle plots illustrating the effect of the number of particle on the shape and penetration of the spray (P_b = 3.0 MPa, t = 3.0 ms). (a) K = 2, N_p = 300; (b) K = 3, N_p = 450; (c) K = 4, N_p = 600; (d) K = 5, N_p = 750.

particles will improve the statistical accuracy of the calculation but it will increase computational time and storage requirements. Figure 6 illustrates the result of varying K. The figure shows particle plots for the same spray ($P_b = 3$ MPa, see Table II) at identical times, for a range of values of K ($K = 2, 3, 4, 5$). It appears that, provided $K > 2$, the dynamics of the spray are not very sensitive to variation in this parameter. This is fortunate because it implies that the present technique is computationally economical since relatively few particles are required for an accurate description. The technique breaks down for $K = 1$ since it is then impossible to model the droplet size distribution (see Section 3.4).

4.4. 45° *Hollow-Cone Spray*

A case of some practical importance is that of sprays with a hollow-cone shape, since such sprays produce improved dispersion. This is also a case that is very difficult, if not impossible, to model using the continuum two-phase approach. In the absence of detailed experimental data, several artificial hollow-cone sprays were computed to illustrate the qualitative features of such sprays. Figure 7 shows the particle plot and the velocity vectors for a monodisperse spray, with droplet radius $r_p = 10\,\mu$, injected into air at approximately atmospheric back pressure ($P_b = 0.1$ MPa), and neglecting particle turbulence. The injection velocity is 100 m/s. The mesh is composed of square cells, 1 mm on a side. The injector is shown in outline in the lower center portion of the particle plot. The scale of the plot is indicated by the fact that the injector is two cells

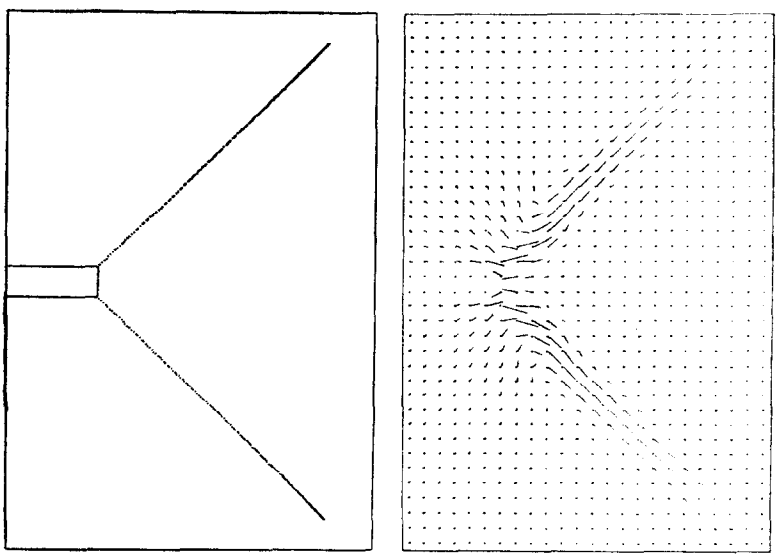

FIG. 7. Velocity vectors and particle plot illustrating a weakly interacting 45° hollow-cone spray ($P_b = 1.1$ MPa, $r_p = 10\,\mu$, $t = 0.3$ ms).

wide and six cells high. The geometry is axisymmetric and the lower boundary represents a solid plate with a free-slip boundary condition. At this low back pressure, and relatively large droplet size, there is little interaction with the gas and the spray preserves its shape, with a small amount of clustering at the tip of the spray. The entrainment of the gas is not large and the gas flow is confined essentially to the vicinity of the spray.

For a smaller droplet size ($r_p = 2.5\,\mu$) at the same back pressure, the interaction with the gas is much stronger, as seen in Fig. 8. The spray penetration has decreased and the shape of the spray is no longer conical, due to the interaction of the droplets with the induced air flow [22]. The velocity vectors show the presence of a vortex near the head of the spray, which curls the spray tip toward the outside of the spray. The induced air flow velocities are much higher and more air is entrained. There also appears to be a region of strong inward flow in the center of the cone near the injector.

When the back pressure is increased, for the same droplet size ($P_b = 3.0$ MPa, $r_p = 2.5\,\mu$), the coupling with the gas becomes very strong, as seen in Fig. 9. Most of the spray momentum is transferred to a larger amount of the gas, with the result that the air flow velocities are lower, and the spray penetration has been slowed further. The velocity vectors show that the gas velocities inside the spray are primarily in the axial direction. This pattern is similar to observed flow patterns from smoke flow visualization studies [23, 24] of hollow-cone sprays.

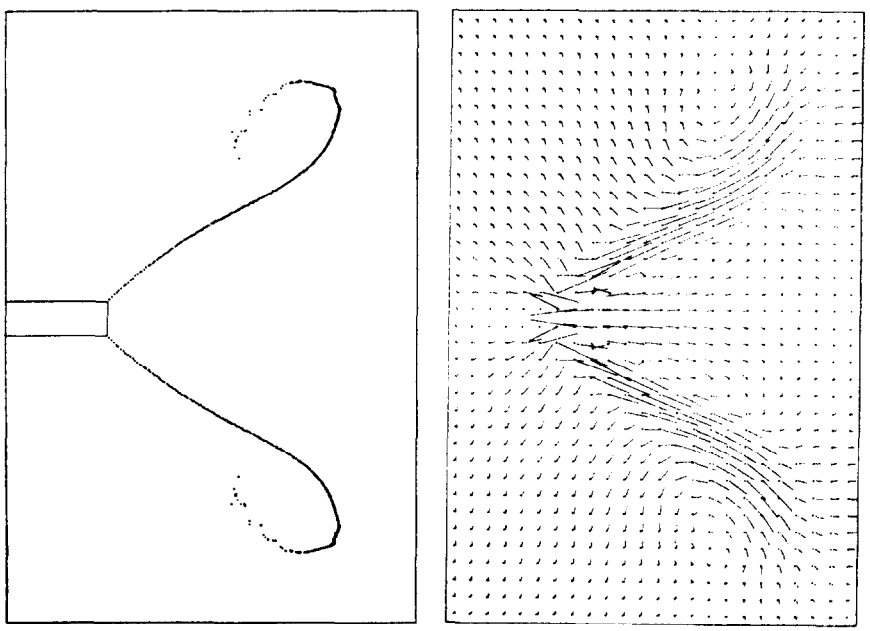

FIG. 8. Velocity vectors and particle plot illustrating a moderately interacting 45° hollow-cone spray ($P_b = 1.1$ MPa, $r_p = 2.5\,\mu$, $t = 0.6$ ms).

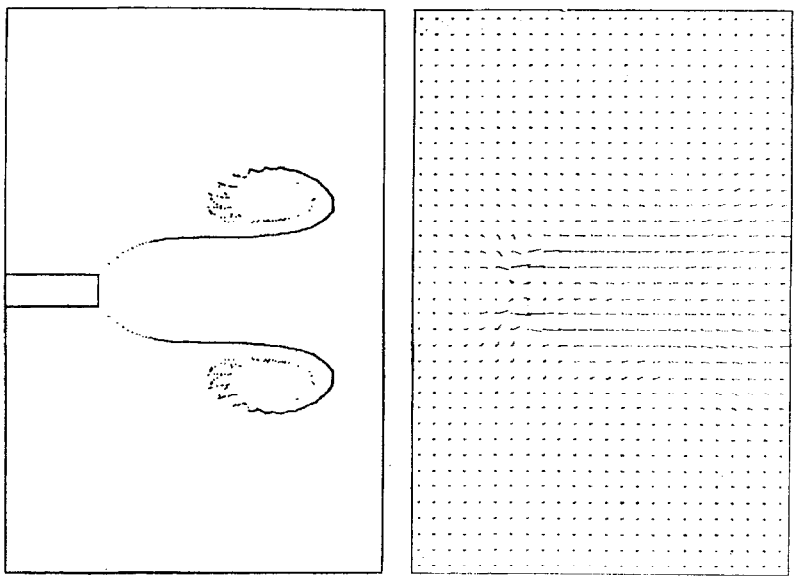

FIG. 9. Velocity vectors and particle plot illustrating a strongly interacting 45° hollow-cone spray (P_b — 3.0 MPa, r_p — 2.5 μ, t = 3.0 ms).

5. DISCUSSION

The numerical technique described has generally been well-behaved except under conditions when particles cluster locally so that the void fraction becomes negative in that cell. This is strictly unphysical since it implies that particles occupy more space than is available. Under these conditions the flow quickly becomes unstable. There are a number of possibilities for modifying the technique to prevent particles from packing closer together than the close-packed limit, for example. However, in practice, especially when particle turbulence provides particle diffusion, this problem rarely arises.

The development of the technique is based on the assumption of noninteracting droplets. While this assumption is bound to fail in the vicinity of the injector, it is not clear whether neglecting this effect will have a significant effect on the subsequent dynamics of the spray, provided reasonable data are available for droplet distributions close to the injection. Clearly, many other approximations are involved, such as the assumption of spherical droplets, as well as the numerical inaccuracies associated with a finite mesh. The penetration curves of Fig. 3 suggest that good practical results can be obtained with the present technique. Much better experimental data than currently available will be necessary to resolve these questions.

APPENDIX: PARTICLE STATISTICS

A fundamental formulation of particle dynamics may be obtained in terms of a Liouville equation for the particle distribution function [9]. This formulation is identical to the well-known spray equation given by Williams [14]. It can be shown that the multifluid equations are equivalent to moments of the spray equation [9]. It is therefore useful to point out the relationship of the present particle formulation to the spray equation.

The spray equation defines the behavior of the droplet distribution function f, which is defined such that

$$dN = f(r, \mathbf{x}, \mathbf{u}_p, t)\, dr\, d\mathbf{x}\, d\mathbf{u}_p \tag{A1}$$

is the average number of droplets of radius r in the interval dr, located at position $\mathbf{x}$ in the volume interval $d\mathbf{x}$, and with velocity $\mathbf{u}_p$ in the interval $d\mathbf{u}_p$, at time t.

In a particular realization, a cloud of droplets at time t, for example, the number of droplets in the small interval Δr, Δx, and $\Delta \mathbf{u}_p$ can be expressed as

$$\Delta N = \int_{\Delta r, \Delta \mathbf{x}, \Delta \mathbf{u}_p} \sum_k \delta(r - r_k)\, \delta(\mathbf{x} - \mathbf{x}_k)\, \delta(\mathbf{u} - \mathbf{u}_{pk})\, dr\, d\mathbf{x}\, d\mathbf{u}_p . \tag{A2}$$

Taking an ensemble average, the average number of droplets is

$$\Delta N = \int_{\Delta r, \Delta \mathbf{x}, \Delta \mathbf{u}_p} < \sum_k \delta(r - r_k)\, \delta(\mathbf{x} - \mathbf{x}_k)\, \delta(\mathbf{u} - \mathbf{u}_{pk}) > dr\, d\mathbf{x}\, d\mathbf{u}_p . \tag{A3}$$

Since the ensemble average is expected to be essentially constant over the small interval Δr, Δx, $\Delta \mathbf{u}_p$, we can take it outside the integral sign, and we obtain

$$\begin{aligned} \Delta N &= < \sum_k \delta(r - r_k)\, \delta(\mathbf{x} - \mathbf{x}_k)\, \delta(\mathbf{u}_p - \mathbf{u}_{pk}) > \int_{\Delta r, \Delta \mathbf{x}, \Delta \mathbf{u}_p} dr\, d\mathbf{x}\, d\mathbf{u}_p \\ &= < \sum_k \delta(r - r_k)\, \delta(\mathbf{x} - \mathbf{x}_k)\, \delta(\mathbf{u}_p - \mathbf{u}_{pk}) > \Delta r\, \Delta \mathbf{x}\, \Delta \mathbf{u}_p . \end{aligned} \tag{A4}$$

Comparing this with Eq. (A1), we can immediately see that in the limit of an infinitesimal volume $\Delta r\, \Delta \mathbf{x}\, \Delta \mathbf{u}_p$

$$f(r, \mathbf{x}, \mathbf{u}_p, t) = < \sum_k \delta(r - r_k)\, \delta(\mathbf{x} - \mathbf{x}_k)\, \delta(\mathbf{u}_p - \mathbf{u}_{pk}) >. \tag{A5}$$

This defines the relationship between the continuum statistical description embodied in the spray equation and the discrete particle realization described in the previous sections.

For modeling purposes, it is not possible to deal with the large numbers of droplets present in an actual spray so that a sampling technique must be employed in which

each single particle represents a characteristic group of particles. This is equivalent to the following "instantaneous" distribution function:

$$f(r, \mathbf{x}, \mathbf{u}_p, t) = \sum_k N_{pk}\delta(r - r_k)\,\delta(\mathbf{x} - \mathbf{x}_k)\,\delta(\mathbf{u}_p - \mathbf{u}_{pk}), \tag{A6}$$

where N_{pk} is the number of identical particles represented by particle k. The number N_{pk} is determined by boundary conditions, and by the constraint.

$$\sum_k N_{pk}m_k = M, \tag{A7}$$

where M is the total mass of particles.

Calculating a large number of realizations to obtain ensemble averages is clearly impractical. Instead, it is possible to substitute volume averages. Referring to Eqs. (A4) and (A5), we see that

$$f(r, \mathbf{x}, \mathbf{u}_p, t) = \langle \sum_k \delta(r - r_k)\,\delta(\mathbf{x} - \mathbf{x}_k)\,\delta(\mathbf{u} - \mathbf{u}_{pk}) \rangle \simeq \frac{\Delta N}{\Delta r\,\Delta \mathbf{x}\,\Delta \mathbf{u}_p}. \tag{A8}$$

where ΔN is the number of particles in the "volume" $\Delta r \Delta \mathbf{x} \Delta \mathbf{u}_p$. The number of particles in the calculation can be increased to improve the approximation. Standard statistical tests can then be performed to evaluate the approximation, if desired. Actually, it will rarely be necessary to evaluate the distribution function directly. However, initial conditions, or boundary conditions, will frequently be most conveniently specified in terms of the distribution functions $f(r, \mathbf{x}, \mathbf{u}_p, 0)$, or $f(r, \mathbf{x}_0, \mathbf{u}_p, t)$, where $\mathbf{x}_0$ are the boundary coordinates. For example, in the spray problem the boundary conditions specifying the injector velocity distribution and droplet size distribution must be provided.

ACKNOWLEDGMENTS

Many helpful discussions with T. D. Butler, and especially J. D. Ramshaw, who contributed the particle injection technique given by Eqs. (3.23) and (3.24), are gratefully acknowledged. Thanks are due to Professor G. L. Borman who pointed out the probable existence of droplet agglomeration in the experiments of Hiroyasu and Kadota. This work was performed under the auspices of the U.S. Department of Energy, Contract W-7405-ENG-36.

REFERENCES

1. R. S. HOTCHKISS AND C. W. HIRT, Particulate Transport in Highly Distorted Three-Dimensional Flow Fields, in Proceedings of the 1972 Summer Simulation Conference, SHARE, San Diego, June 14–16, 1972 (also Los Alamos Scientific Laboratory Preprint LA-DC-72-364, 1972).
2. W. H. GAUVIN, S. KATTA, AND F. H. KNELMAN, *Internat. J. Multiphase Flow*, **1** (1975), 793–816.
3. C. K. WESTBROOK, Three Dimensional Numerical Modeling of Liquid Fuel Sprays, in Sixteenth Symposium (International) on Combustion, The Combustion Institute, Pittsburgh, 1976.

4. D. ADLER AND W. T. LYN, *Internat. J. Heat Mass Transfer* **14** (1971), 793–812.
5. J. RIFE AND J. B. HEYWOOD, "Photographic and Performance Studies of Diesel Combustion With a Rapid Compression Machine," SAE paper 740948, 1974.
6. G. N. ABRAMOVICH, "The Theory of Turbulent Jets," M.I.T. Press, Cambridge, 1963.
7. W. S. CHIU, S. M. SHADED, AND W. T. LYN, "A Transient Spray Mixing Model for Diesel Combustion," SAE paper 769128, 1976.
8. F. H. HARLOW AND A. A. AMSDEN, *J. Comput. Phys.* **17** (1975), 19–52.
9. J. R. TRAVIS, F. H. HARLOW, AND A. A. AMSDEN, *Nucl. Sci. Engng.* **61** (1976), 1–10.
10. L. C. HASELMAN AND C. K. WESTBROOK, "A Theoretical Model for Fuel Injection in Stratified Charge Engines," SAE paper 780138, 1978.
11. A. A. AMSDEN AND C. W. HIRT, "YAQUI: An Arbitrary Lagrangian-Eulerian Computer Program for Fluid Flow at All Speeds," Los Alamos Scientific Laboratory Report LA-5100, 1973.
12. C. T. CROWE, M. P. SHARMA, AND D. E. STOCK, *Trans. ASME ,J. Fluids Engng.* (1977), 325–332.
13. T. PEARCEY AND G. W. HILL, *Austral. J. Phys.* **9** (1955), 19–30.
14. F. A. WILLIAMS, "Combustion Theory," Addison–Wesley, Reading, Mass., 1965.
15. C. W. HIRT, B. D. NICHOLS, AND N. C. ROMERO, "SOLA—A Numerical Solution Algorithm for Transient Fluid Flows," Los Alamos Scientific Laboratory Report LA-5852, 1975.
16. C. W. HIRT AND J. L. COOK, *J. Comput. Phys.* **10** (1972), 324–350.
17. R. D. REITZ, "Atomization and Other Breakup Regimes of a Liquid Jet," Thesis 1375-T, Princeton University, 1978.
18. L. G. MARGOLIN, "Turbulent Diffusion of Small Particles," Los Alamos Scientific Laboratory Report LA-7040-T, 1977.
19. H. HIROYASU AND T. KADOTA, "Fuel Droplet Size Distribution in Diesel Combustion Chamber," SAE paper 740715, 1974.
20. H. HIROYASU AND T. KADOTA, "Fuel Droplet Size Distribution in Diesel Combustion Chamber," *Bull. Jap. Soc. Mech. Eng.* **19** (1976), 1064–1072.
21. H. SCHLICHTING, "Boundary-Layer Theory," 6th edition, McGraw–Hill, New York, 1968.
22. P. H. ROTHE AND J. A. BLOCK, *Internat. J. Multiphase Flow* **3** (1977), 263–272.
23. H. BINARD AND W. E. RANZ, "Induced Air Flows in Fuel Sprays," ASME paper 58-A-284, 1958.
24. F. G. S. BENATT AND P. EISENKLAM, *J. Inst. Fuel.* **42** (1969), 309–315.